Removal of Cd^{2+} in water by FeSO$_4$ magnetic modified eggshell adsorbent

Dekang Meng[a,b], Xiangyi Gong[a,b],*, Zhang Peng[b], Zeya Wang[b], Dajun Ren[b]

[a]*Hubei Key Laboratory for Efficient Utilization and Agglomeration of Metallurgic Mineral Resources, Wuhan University of Science and Technology, Wuhan 430081, China, emails: gxywust@163.com (X. Gong), 295944628@qq.com (D. Meng)*
[b]*School of Resource and Environmental Engineering, Wuhan University of Science and Technology, Wuhan 430081, China, emails: pengzhang1995@163.com (Z. Peng), 13507282990@139.com (Z. Wang), dj_ren@163.com (D. Ren)*

ABSTRACT

Cadmium content in the environment if exceeded would cause significant harm to human health. In this study, a FeSO$_4$ and magnetism modified method was used to prepare an eggshell magnetic adsorbent (BC-FM) to adsorb cadmium in water. Through material characterization and a series of experiments on the adsorption of Cd^{2+}, the adsorption characteristics and mechanism were studied. Characterization showed that the specific surface area and total pore volume of BC-FM were increased after modification, and the magnetic functional group Fe–O (γ-Fe$_2$O$_3$) was successfully attached to the surface of BC-FM. Compared with the original adsorbent (BC), the adsorption capacity of BC-FM was greatly improved, and their equilibrium adsorption capacities were respectively 4.82 and 47.33 mg g^{-1}. Pseudo-second-order kinetics equation and Langmuir adsorption isotherm fit the adsorption process well. pH and the presence of Mg^{2+}, Pb^{2+}, Cu^{2+} and Zn^{2+} had great influence on its capacity to absorb Cd^{2+}. The main adsorption mechanisms were surface adsorption, strong electrostatic interaction and complexation of oxygen-containing functional groups and compounds containing Fe. BC-FM was easy to separate from water and has good reuse performance. After 5 cycles of adsorption–desorption, the adsorption capacity of Cd^{2+} still reached 81.9% of that of fresh adsorbent.

Keywords: Eggshell; Low-cost adsorbent; Magnetic modification; Cadmium

1. Introduction

Cadmium is a toxic heavy metal widely present in the environment. Long-term exposure to cadmium or ingestion of cadmium, can cause serious harm to human health. Cadmium can cause a variety of diseases, such as liver and kidney damage [1], osteomalacia [2], reproductive system disorders [3], damage to the human immune system and cancer [4,5]. Cadmium mainly exists in zinc deposits and cadmium-rich sedimentary rocks in the form of cadmium sulfide. Volcanic eruptions will cause it to enter the ground environment [6]. Artificial mining and industrial processing had greatly increased the cadmium content in human living environment [7]. Cadmium can diffuse into soil and water by discharge of industrial wastewater. Moreover, it will be absorbed by plants, and further enters the human body through the food chain. Therefore, the removal of cadmium in wastewater is an urgent problem to be solved.

In recent years, a variety of technologies are being studied to remove cadmium from sewage or have been used in actual treatment, such as chemical precipitation, ion exchange, electrokinetic repair, membrane separation, and adsorption [8]. Among them, adsorption technology has attracted much attention due to its economy, effectiveness,

* Corresponding author.

and the recyclability of adsorbents [9–11]. Low-cost sorbents made from agricultural and domestic waste can help remove refractory pollutants during wastewater treatment. For example, biochar, as one of them, has received a lot of attention due to its effectiveness, practicality, wide sources [12,13].

High temperature pyrolysis and carbonization are common methods for making these adsorbents. Due to different raw materials, carbonization temperature and process conditions, the structure and properties of different adsorbent vary greatly. Raw material is an important factor affecting the structure and properties of these low-cost absorbents. Hydroxyapatite synthesized from eggshell waste is an efficient and low-cost adsorbent, which can be used to adsorb harmful metals in water [14]. Furthermore, eggs are a common food staple, about 65.5 million tons of eggs are produced worldwide each year [15], that translates to nearly 7.2 million tons of eggshell waste each year [16], and how to dispose of these wastes is a problem of great significance. Eggshell can be utilized as it has a composition of 94% calcium carbonate, 1% magnesium carbonate, 1% calcium phosphate and 4% organic matter [17]. Eggshells, including those without and after high temperature treatment, have been studied as adsorbents for removing pollutants from water, and the adsorption effect was good [18,19]. Adsorbents prepared by pyrolysis of raw materials alone are often difficult to balance removal efficiency and economic benefits. Therefore, it is a problem that researchers have been working on for a long time to improve the removal efficiency of contaminant by modification of original absorbents.

Iron modification can effectively improve the adsorption capacity of absorbents for heavy metals in water, and the modified material is easy to recycle due to the magnetism of iron, which is a promising modification method [20]. Currently, researchers have prepared many types of iron-based absorbents, including zero-valent iron [21], iron oxides [22], iron sulfides [23], iron salts [24]. There are few studies on magnetic modification of eggshell absorbent, and its adsorption performance, mechanism and sustainability need to be further explored.

Therefore, the purpose of this study is to (1) prepare a $FeSO_4$-magnetically modified eggshell absorbent (BC-FM) by chemical co-precipitation (using Fe^{3+}/Fe^{2+} solution) on the basis of modification of $FeSO_4$ to remove Cd^{2+} in water; (2) analyze the adsorption characteristics and mechanism of Cd^{2+} on $FeSO_4$-magnetically modified eggshell absorbent by physical and chemical characterization methods, kinetics, and isothermal adsorption experiments; (3) explore the influence of pH and other factors on the adsorption of Cd^{2+} by $FeSO_4$-magnetically modified eggshell absorbent, and explored its regeneration performance through repeated adsorption and desorption experiments.

2. Materials and methods

2.1. Chemical reagents

$FeSO_4·7H_2O$, $FeCl_3·6H_2O$, NaOH, $CdCl_2·2.5H_2O$, HNO_3, NaCl, Na_2CO_3, Na_2SO_4, $Na_3PO_4·12H_2O$, $NaNO_3$, $Mg(NO_3)_2·6H_2O$, $Pb(NO_3)_2$, $Cu(NO_3)_2·3H_2O$, $Zn(NO_3)_2·6H_2O$ were all analytical reagent grade and purchased from Sinopharm

Chemical Reagent Co., Ltd., (China); The experimental water was pure water prepared by a water purifier; the Cd^{2+} solution was prepared with $CdCl_2·2.5H_2O$ and 0.01 mol L^{-1} $NaNO_3$ solution as the background solution.

2.2. Preparation of absorbents

2.2.1. Preparation of original eggshell adsorbent

The eggshell with the inner lining removed was washed, dried, milled and pass through a 100-mesh sieve. Eggshell powder (30 g) was transported into the tube furnace (OTF-1200X, Hefei, China) under nitrogen atmosphere with a heating rate of 10°C/min from the room temperature to 500°C and continuous pyrolysis at this temperature for 120 min. After cooling to room temperature, the material was removed and stored under dry conditions. The adsorbent produced by the above method was named BC.

2.2.2. Preparation of $FeSO_4$ modified eggshell adsorbent

3.2 g of $FeSO_4·7H_2O$ were dissolved in 50 mL of deionized water and stirred for 30 min. At the same time, 3.2 g of BC were put in 50 mL of deionized water and stirred for 30 min. The above two mixtures were mixed and treated with ultrasound for 30 min [25]. The resulting mixture was washed with deionized water until neutral, filtered and dried at 80°C. The adsorbent produced by the above method was named BC-F.

2.2.3. Preparation of $FeSO_4$-magnetic modified eggshell adsorbent

3.0 g of BC-F were put in 30 mL deionized water, 3.0 g of $FeCl_3·6H_2O$ and 1.4 g of $FeSO_4·7H_2O$ were dissolved in 70 mL deionized water, and then dissolved the above two mixes, stirred for 20 min. The NaOH solution was added to the mixture by drops until the pH was 10. Stirred the mixture for 60 min and let it sit for another hour [26]. The resulting mixture was washed with deionized water until neutral, filtered and dried at 80°C. The adsorbent produced by the above method was named BC-FM.

2.3. Characterization of absorbents

The main surface functional group characteristics of the adsorbents before and after modification were measured by Fourier-transform infrared spectroscopy (FTIR) (Thermo Scientific Nicolet 6700, USA). The microscopic features of the samples before and after experiments were characterized by a scanning electron microscope (Apreo S HiVac, Thermo Fisher Scientific, USA; TESCAN MIRA 4, TESCAN, CZE) equipped with energy-dispersive X-ray spectrometer (EDS) patterns. The characteristics of the specific surface area and pore structure are measured by fully automatic specific surface and porosity analyzer (ASAP 2460, Micromeritics, USA). The X-ray diffraction (XRD) analysis was conducted to identify crystallographic structures of the samples using an X-ray diffractometer (Bruker D8 advance, Bruker, GER). The magnetic

property of sample was characterized by a vibrating sample magnetometer (Lakeshore7404, Lake shore, USA).

2.4. Adsorption experiments

0.05 g of adsorbent (BC, BC-F or BC-FM) and 50 mL Cd^{2+} solution were added into a 100 mL conical flask. It was shaken on a thermostatic oscillator at the condition of 200 rpm and 25°C. After the adsorption process, the adsorbent was separated by filtration with the use of a 0.45 μm syringe filter. Except for isothermal adsorption, the concentrations of Cd^{2+} solution in other adsorption experiments were all 50 mg L^{-1}.

The adsorption kinetics experiments were conducted within 1,440 min (15, 30, 60, 90, 120, 240, 360, 480, 600, 720, 840, and 1,440 min). The adsorption isotherm experiments were established with Cd^{2+} concentrations of 30 ~ 80 mg L^{-1} (30, 40, 50, 60, 70, 80 mg L^{-1}) after 8 h oscillation. The isotherms were obtained after pH influence experiment, ion strength influence experiment and adsorption kinetics.

For the influence of ionic strength on the Cd^{2+} adsorption of BC-FM, the concentration of Na^{+} was respectively controlled to 0.01, 0.02, 0.03, 0.04, 0.05 and 0.06 mol L^{-1}. For the influence of dosage of adsorbent, the dosage of BC-FM was respectively controlled to 0.01, 0.02, 0.03, 0.04, 0.05 and 0.06 g. For the influence of concomitant ions, 0.01 mol L^{-1} of Cl^{-}, CO_3^{2-}, PO_4^{3-}, SO_4^{2-}, Mg^{2+}, Pb^{2+}, Cu^{2+}, and Zn^{2+} were respectively added into the Cd^{2+} solution. For the influence of pH value, the pH of Cd^{2+} solution was respectively controlled to 1, 2, 3, 4, 5 and 6. The pH of the solutions was adjusted by adding 0.1 M NaOH or 0.1 M HNO_3 solution.

The experiments to evaluate the recycling capacity of adsorbents were carried out under the conditions of 0.05 g (BC-FM) and 50 mL Cd^{2+} solution. The above mixture was oscillated at 25°C and 200 rpm for 8 h, and then the adsorbents were separated by filter. Subsequently, the adsorbents were dried in an oven at 70°C. Then 0.05 g of dried adsorbent was used for desorption by oscillation under the same conditions. The above process was cycled for 5 times.

In all adsorption experiments, three groups of parallel experiments were set.

2.5. Analysis methods

The concentration of Cd^{2+} was detected with flame atomic absorption spectrophotometer (novAA350). The adsorption capacity and removal percentage of Cd^{2+} by the adsorbent were calculated according to Eqs. (1) and (2):

$$q_t = \frac{(C_0 - C_t)V}{m} \tag{1}$$

$$\eta = \frac{C_0 - C_t}{C_0} \tag{2}$$

where q_t is the amount of Cd^{2+} adsorbed at the time of adsorption t (mg g^{-1}); V is the volume of the solution (L); η is the removal percentage of Cd^{2+}; m is the mass of adsorbent (g); C_0 is the initial concentration of Cd^{2+} (mg L^{-1}); C_e is the equilibrium concentration of Cd^{2+} (mg L^{-1}).

2.6. Adsorption model

Adsorption kinetic model: pseudo-first-order and pseudo-second-order models and the Weber–Morris kinetic model were used to fit the adsorption experimental data. The specific equations were as follows, where the pseudo-first-order kinetic model equation was as Eq. (3), the pseudo-second-order kinetic model equation was as Eq. (4), and the Weber–Morris kinetic model equation was as Eq. (5).

$$q_t = q_e\left[1 - \exp(-k_1 t)\right] \tag{3}$$

$$\frac{t}{q_t} = \frac{1}{k_2 q_e^2} + \frac{t}{q_e} \tag{4}$$

$$q_t = k_{ip} t^{0.5} + C \tag{5}$$

where q_m is the equilibrium adsorption capacity (mg g^{-1}); k_1 is the rate constant of the pseudo-first-order kinetic model (min^{-1}); k_2 is the rate constant of the pseudo-second-order kinetic model (g mg^{-1} min^{-1}); k_{ip} is the diffusion rate constant within the particle (mg g^{-1} min$^{-1/2}$); t is the adsorption time (min).

Isothermal adsorption model: Langmuir model and Freundlich model were used to fit and analyze the data. The equations were as follows, where the Langmuir model equation was as Eq. (6), and the Freundlich model equation was as Eq. (7).

$$q_e = \frac{q_m K_L C_e}{1 + K_L C_e} \tag{6}$$

$$q_e = K_F C_e^{\frac{1}{n}} \tag{7}$$

where q_e is the equilibrium adsorption capacity (mg g^{-1}); q_m is the saturated adsorption capacity (mg g^{-1}); C_e is the concentration of Cd^{2+} when the adsorption reaches equilibrium (mg L^{-1}); K_L is the Langmuir adsorption coefficient; K_F is the Freundlich adsorption coefficient.

3. Results and analysis

3.1. Characteristics of the original and modified adsorbent

Fig. 1 shows the scanning electron microscope images (SEM) of BC, BC-F and BC-FM. BC (a, b) retained part of the eggshell calcium carbonate massive structure. Its surface was relatively flat, and there were some fine pores and cracks; After $FeSO_4$ modification, the surface of BC-F (c, d) was disintegrated and collapsed. Its particle size was significantly smaller than that of BC, and a lot of flocculent structures similar to coral reef were added, from which many needle-like synapses were diffracted; Compared with BC, the particle size of BC-FM sample (e, f) was also further reduced, the surface was similar to foam, rough and fluffy, and the microstructure of pores becomes irregular. It could be inferred that the specific surface area of BC-F and BC-FM were increased compared with BC. That might create more adsorption sites. The morphology
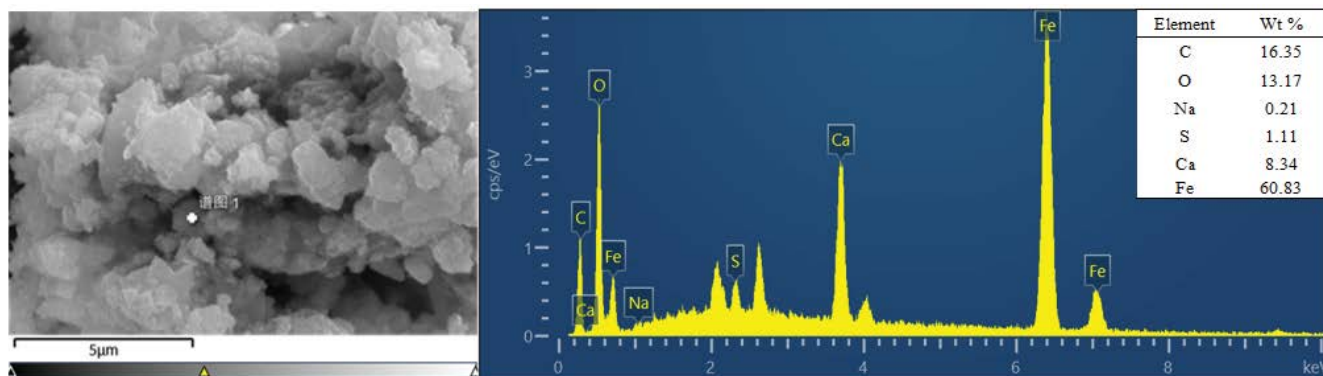
Fig. 1. SEM-EDS spectra of BC-FM under magnifications of 10,000×.

and chemical composition of BC-FM determined by SEM-EDX (Fig. 2) proved the existence of iron oxide (Fe–O) on the surface of it.

The N_2 adsorption–desorption isotherms of the samples before and after modification were shown in Fig. 3a and b. According to the nitrogen adsorption isotherms of IUPAC, they showed a mixture of type II and type IV with the H_3 hysteresis loop. Although the nitrogen adsorption volume of the two materials increased at the low-pressure end, the curve was gently rather than drastically inclined to the *y*-axis, which indicated that the pore structure was probably not dominated by micropores [27]. The desorption isotherm of BC was not overlapped or parallel with its adsorption isotherms. In the range of P/P_0 = 0.5–1.0, the slope of desorption isotherm increased obviously and H_3 hysteresis loop appeared in the isotherms of BC and BC-FM, which indicated that there were mesoporous or macroporous structures such as plate slit structure, crack structure and wedge structure in BC and BC-FM. These were consistent with SEM results.

The pore structure of the two materials was mainly distributed in the mesoporous range, and the pore size was close to the micropore size (Fig. 3c, d and Table 1), which was consistent with the analysis of N_2 adsorption–desorption isotherm. Larger pore size was conducive to the diffusion of macromolecular heavy metal ions in the adsorbent pores. In addition, the specific surface area and pore volume of BC-FM were respectively about 15 and 10 times of that of BC. And that might be due to the formation of iron oxides [28].

The X-ray diffraction patterns of BC, BC-F and BC-FM was displayed in Fig. 3e. For BC-FM, various peaks at 30.24° (220), 35.63° (311), 43.28° (400), 53.73° (422), 57.27° (511) and 62.92° (440) (2θ) were characteristics of γ-Fe_2O_3 that was described with the standard powder diffraction file (PDF 39-1346), and proved the existence of maghemite on the surface of BC-FM. The highest peak at 29.4° (2θ) and other shorter peaks corresponded to the peak of calcite (PDF 47-1743) as $CaCO_3$. The XRD pattern of BC-F also confirmed the adhesion of $FeSO_4$ on its surface (PDF 19-0632) (data not shown due to the low peak).

Fig. 3f shows the FTIR spectra of BC, BC-F, BC-FM before and after the adsorption of Cd^{2+}. The characteristic peak of 3,409–3,458 cm^{-1} was the stretching vibration of hydroxyl (–OH), which indicated the existence of alcohol or phenol or organic acid. The higher peak intensity of BC-FM than that of BC and BC-F indicated the higher content of –OH in BC-FM. 2,877 cm^{-1} was the asymmetric stretching of saturated C–H, and 1,799 cm^{-1} was related to the stretching vibration of C=O. The peak at 1,625 cm^{-1} was due to the stretching vibration of C=C. The strong absorption peak at 1,425 cm^{-1} represented CO_3^{2-} [29], which resulted from the rich $CaCO_3$ in eggshell. The weak peak of BC-F and BC-FM at this point resulted from the fact that Fe^{2+} and Fe^{3+} would react with $CaCO_3$ in water and convert to $Fe(OH)_3$ and Fe–O.

$$3CO_3^{2-} + 2Fe^{3+} + 3H_2O \rightleftharpoons Fe(OH)_3(s) + CO_2(g) \qquad (8)$$

$$CO_3^{2-} + Fe^{2+} \rightleftharpoons FeCO_3(s) \qquad (9)$$

$$FeCO_3(heating) \rightleftharpoons FeO + CO_2(g) \qquad (10)$$
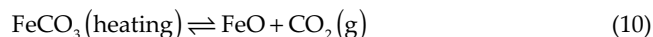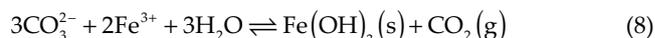
The new peak of BC-FM at 1,143 cm^{-1} was the stretching vibration of C–O, indicating the existence of esters, ethers and alcohols. The sharp absorption peak at 875 cm^{-1} could be attributed to the swing of =CH_2. The new absorption peak of BC-FM at 600 cm^{-1} was caused by Fe–O [30]. The spectra of BC and BC-F changed little before and after adsorption, suggesting that the complexation of oxygen-containing functional groups might not be the main adsorption mechanism, and the decrease of peak height at 1,425 cm^{-1} could be attributed to the hydrolysis of CO_3^{2-}. In addition, comparing the infrared spectra of BC-FM before and after adsorption, it could be found that the main difference lied in the weakened C–O stretching vibration peak after adsorption and its position deviation, indicating BC-FM might have complexation and generate stable coordination compounds in the process of adsorption of Cd^{2+} [31]. Moreover, the shift of the Fe–O peak at 600 cm^{-1} illustrated that the Fe–O group was involved in the adsorption of Cd^{2+} by the adsorbent.

3.2. Adsorption kinetics

The adsorption capacity of three adsorbents for Cd^{2+} presented a rapid growth trend in the period of 0–240 min, and tended to be stable after 240 min (Fig. 4a). At each
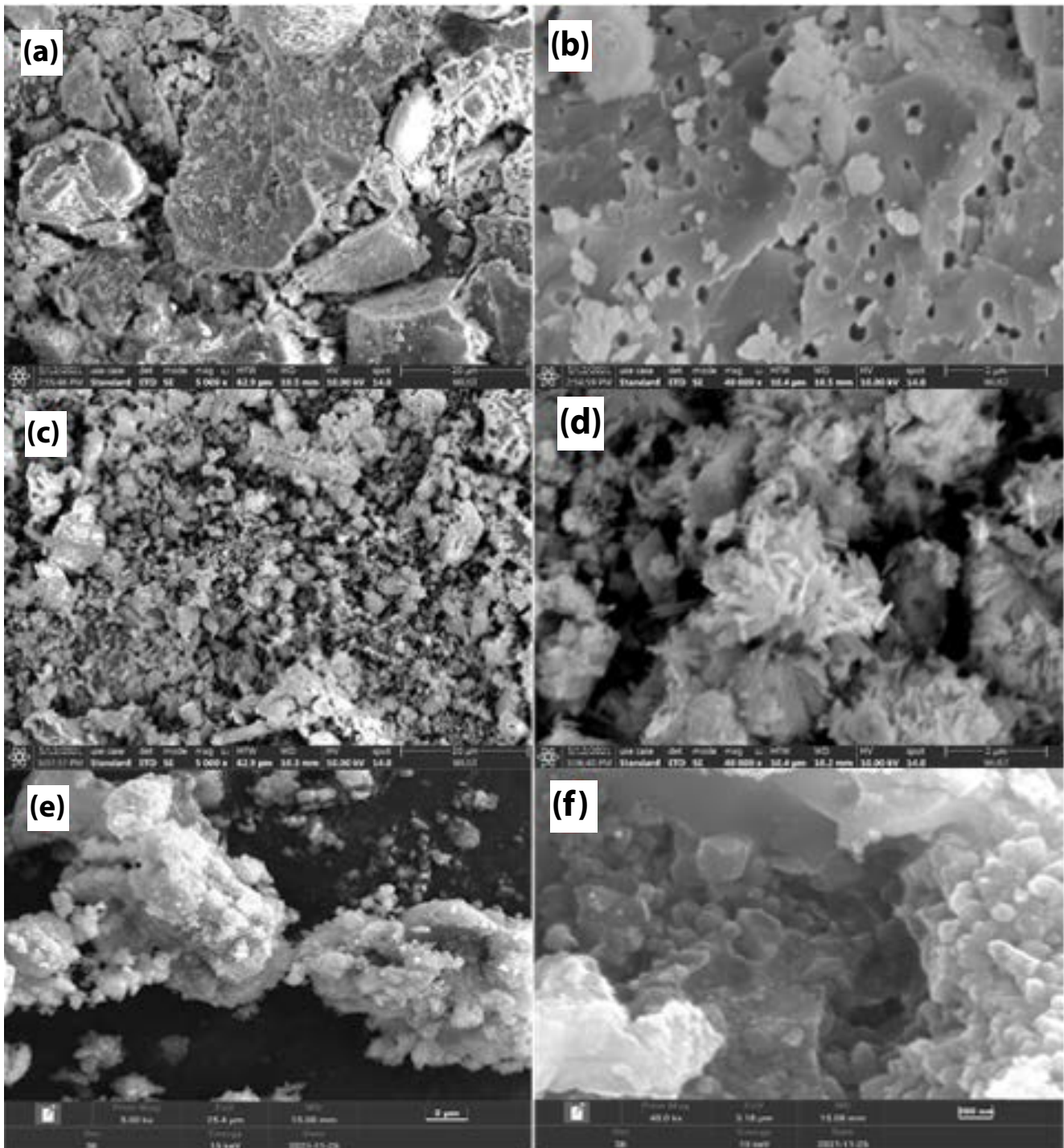
Fig. 2. SEM images of BC (a, b), BC-F (c, d) and BC-FM (e, f).

time point, the adsorption capacity of BC-F for Cd²⁺ was higher than that of BC, while the adsorption capacity of BC-FM for Cd²⁺ was much higher than that of BC and BC-F. The equilibrium adsorption capacities of BC, BC-F and BC-FM were respectively 4.82, 15.60 and 47.33 mg g⁻¹, which indicated that the adsorption effect of modified adsorbent was better than that of original adsorbent. It was

mainly because BC-FM had larger specific surface area and more adsorption sites than BC according to the results of SEM and Brunauer–Emmett–Teller (BET). At the beginning of adsorption, the adsorption capacity increased rapidly because the adsorption mainly occurred on the external surface of adsorbent. With the increase of reaction time, the active sites were occupied, and Cd²⁺ gradually diffused
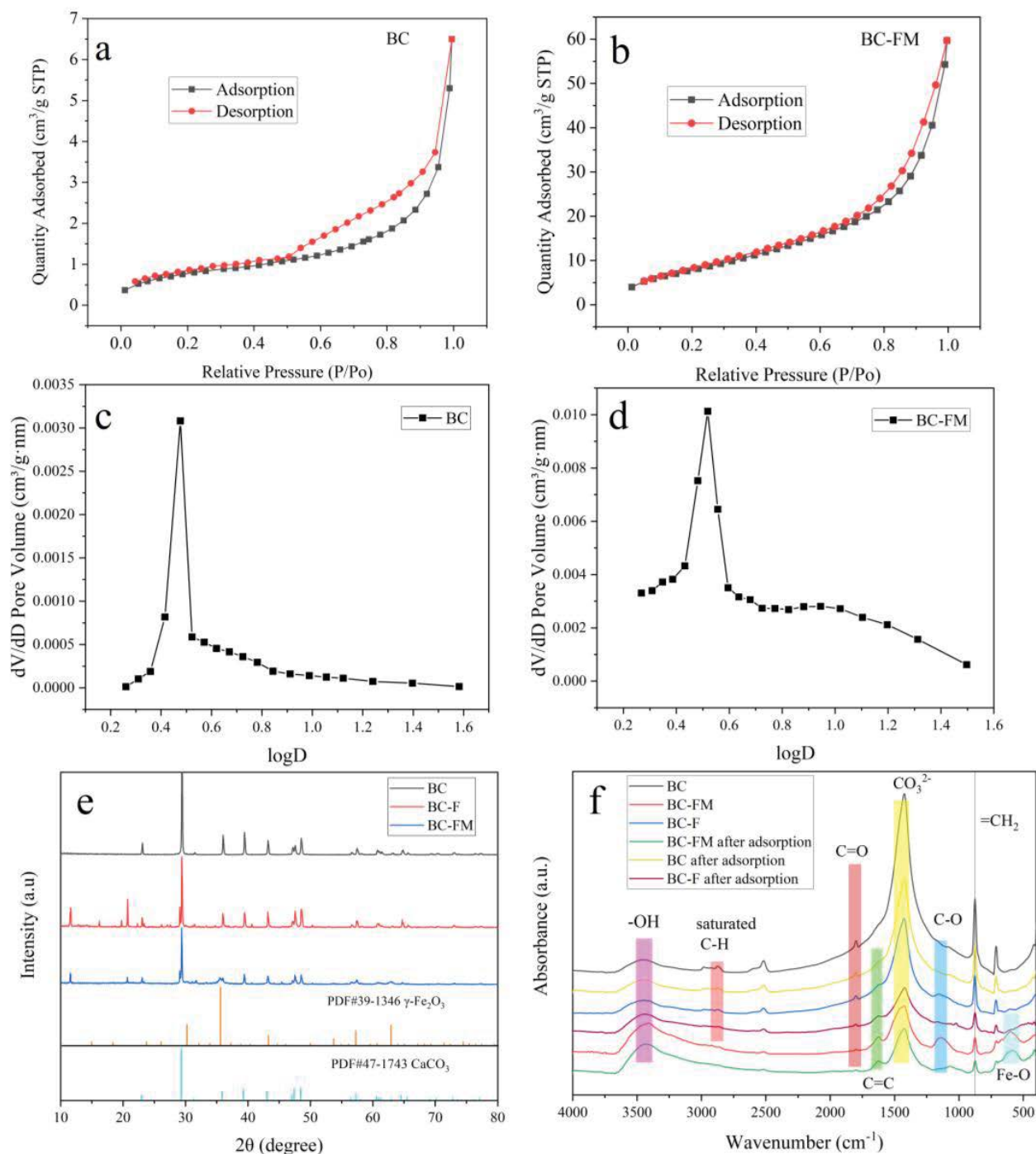
Fig. 3. The N_2 adsorption–desorption isotherms (a, b) and the pore size distribution (c, d) of BC and BC-FM; X-ray diffraction (XRD) pattern of samples and standard XRD pattern of γ-Fe_2O_3 and $CaCO_3$ (e); FTIR spectra of BC, BC-F, and BC-FM before and after absorption (f).

Table 1
Pore structure parameter of BC and BC-FM

Samples	Specific surface area ($m^2\ g^{-1}$)	Total pore volume ($cm^3\ g^{-1}$)	Most probable pore size (nm)
BC	2.866	0.0051	2.995
BC-FM	30.18	0.0627	3.299

into the carbon pores, further reacting with the internal active sites of the adsorbent. Finally, the adsorption process reached equilibrium state relatively slowly [32].

Pseudo-first-order and pseudo-second-order models were used to fit the experimental data (Fig. 4a), and the relevant fitting parameters are shown in Table 2 [33]. Apparently, pseudo-second-order model could better fit the adsorption kinetics of Cd^{2+} by BC and BC-F, while the pseudo-first-order model and pseudo-second-order model were both suitable for describing the adsorption of Cd^{2+}
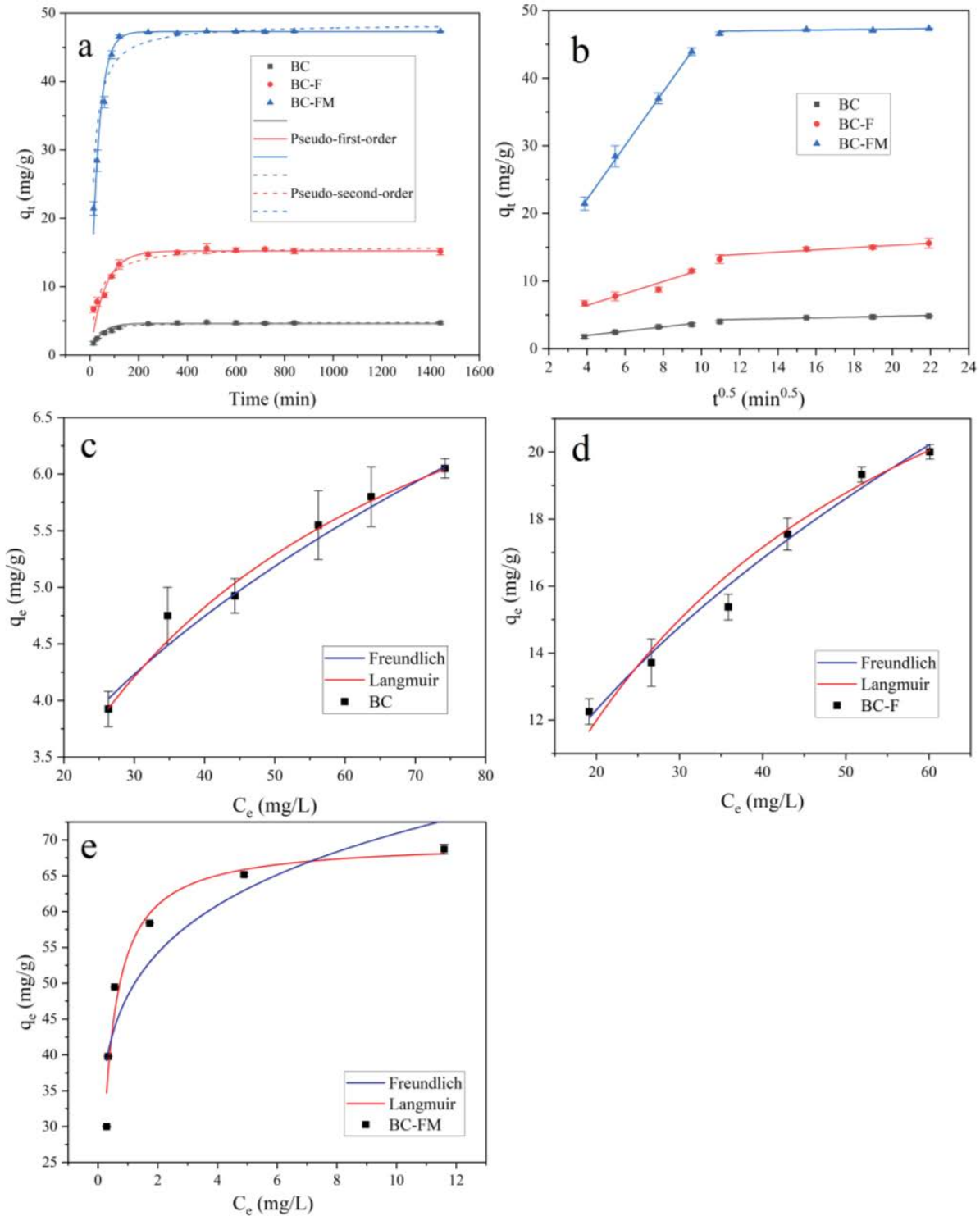
Fig. 4. Adsorption kinetics for Cd^{2+} by BC, BC-F, and BC-FM (a) (*T*: 25°C; pH: 6), fitting curves of Weber–Morris model (b), fitting curves of Langmuir and Freundlich isothermal models (c–e) (*T*: 25°C; pH: 6).

Table 2
Parameters of adsorption kinetics

Adsorbent	Pseudo-first-order equation			Pseudo-second-order equation		
	q_e (mg g^{-1})	k_1 (min^{-1})	R_1^2	q_e (mg g^{-1})	k_2 (g mg^{-1} min^{-1})	R_2^2
BC	4.66 (±0.0895)	0.0211 (±0.0019)	0.946	4.96 (±0.0574)	0.0067 (±0.0005)	0.986
BC-F	15.09 (±0.4413)	0.0194 (±0.0026)	0.876	16.04 (±0.3953)	0.0020 (±0.0003)	0.937
BC-FM	47.06 (±0.5392)	0.0318 (±0.0020)	0.969	49.49 (±0.7916)	0.0011 (±0.0001)	0.955

by BC-FM, indicating that the adsorption kinetics of Cd^{2+} by BC and BC-F was affected by chemical mechanism, and the adsorption of Cd^{2+} by BC-FM was affected by both chemical and non-chemical mechanisms [34].

In order to further determine the adsorption mechanism of Cd^{2+} on the material, the Weber–Morris kinetic model was used to fit the experimental results (Fig. 4b). Since the adsorption reached equilibrium at 480 min, the adsorption data from 0 to 480 min were used for fitting. The related parameters are shown in Table 3, and R^2 was the correlation coefficient. For the three adsorbents, the adsorption fitting curve could be divided into two stages. In the first stage, the slope of the straight line was larger and the adsorption rate was faster, which was the stage of liquid film diffusion; The second stage was the intra particle diffusion stage. In this stage, the adsorption on the adsorbent surface was basically completed, and the C value was higher than the corresponding value in the first stage, reflecting that the boundary layer resistance increased and the adsorption rate gradually decreased. That meant the intra particle diffusion was the main speed limiting step of adsorption on the adsorbent [35]. In addition, there was a good linear relationship between q_t and $t^{0.5}$ in the first and second stage, while the fitting curves did not pass through the origin, indicating that the intra particle diffusion was not the only rate controlling factor and the extra particle diffusion might also affect the rate of adsorption [34].

3.3. Adsorption isotherms

The adsorbed Cd^{2+} contents in three adsorbents increased with the increase of Cd^{2+} concentration in the

solution, but the increasing rates were gradually decreased. Langmuir and Freundlich models were used to fit the data (Fig. 4c–e and Table 4). The adsorption capacity of BC-F for Cd^{2+} was higher than that of BC, while the adsorption capacity of BC-FM for Cd^{2+} was much higher than that of BC and BC-F. The R^2 values of Freundlich model of BC and BC-F were higher than those of Langmuir model, showing that the Freundlich model fitted the adsorption data better than the Langmuir model. This indicated that Cd^{2+} might be mainly affected by multilayer physical adsorption; For BC-FM, the R^2 of Langmuir model (0.953) was higher than that of Freundlich model (0.815), and there was a big difference between the two fitting curves. Therefore, the Langmuir model could better fit the adsorption process of the adsorbent for Cd^{2+} in solution, indicating that the adsorption process of BC-FM for Cd^{2+} was monolayer adsorption, and the distribution of active adsorption sites was irregular. In addition, in the Freundlich model, the larger the n value, the greater the adsorption force of the adsorbent on heavy metal ions. The n value of BC-FM was higher than that of BC and BC-F, which could fully prove that the adsorption capacity of the modified materials for Cd^{2+} was significantly improved.

3.4. Influencing factors of adsorption effect

The removal percentage of Cd^{2+} increased rapidly as the dosage increased from 0.2 to 1.0 g L^{-1}, and then remained above 95% until the dosage reached 1.2 g L^{-1} (Fig. 5c). However, the removal capacity of Cd^{2+} was different from the removal percentage, which firstly increased and then declined with the largest value of 64.82 mg g^{-1} at the dosage

Table 3
Fitting parameters of Weber–Morris model

Adsorbent	Step 1			Step 2		
	k_{ip} (mg g^{-1} min$^{-1/2}$)	C (mg g^{-1})	R^2	k_{ip} (mg g^{-1} min$^{-1/2}$)	C (mg g^{-1})	R^2
BC	0.327 (±0.0328)	0.60 (±0.2293)	0.970	0.071 (±0.0172)	3.34 (±0.2975)	0.843
BC-F	0.800 (±0.1661)	3.36 (±1.1601)	0.881	0.205 (±0.0382)	11.20 (±0.6616)	0.902
BC-FM	3.969 (±0.0764)	6.32 (±0.5332)	0.999	0.060 (±0.0236)	46.02 (±0.4094)	0.648

Table 4
Fitting parameters of isothermal adsorption models

Adsorbent	Langmuir model			Freundlich model		
	q_m (mg g^{-1})	K_L (L mg^{-1})	R^2	K_F (mg$^{1-1/n}$ g^{-1} L$^{1/n}$)	$1/n$	R^2
BC	8.444 (±0.3884)	0.0340 (±0.0042)	0.976	1.1630 (±0.1490)	0.3861 (±0.0334)	0.994
BC-F	30.051 (±2.0143)	0.0327 (±0.0057)	0.963	3.0668 (±0.4242)	0.4604 (±0.0341)	0.981
BC-FM	69.769 (±2.4452)	3.4453 (±0.5171)	0.953	48.3111 (±2.8782)	0.1667 (±0.0357)	0.815

of 0.6 g L^{-1}. In conclusion, within a certain range, the adsorbent dosage had a great influence on the adsorption effect of BC-FM on Cd^{2+}, and the increase of the dosage of BC-FM would significantly enhance the adsorption effect of Cd^{2+} and improve the removal percentage. In order to save the amount of adsorbent and give full play to the removal capacity of BC-FM, the best dosage should be 0.6 g L^{-1}.

The removal percentage of Cd^{2+} by BC-FM decreased with the improving of ionic strength in the solution (Fig. 5a). The change relationship was basically linear. When the ionic strength was 0.01 mol L^{-1}, the removal percentage of Cd^{2+} by BC-FM was 98.74%. When the ionic strength was 0.06 mol L^{-1}, the removal percentage drops to 82.12%. This might be due to the competitive adsorption of Na$^+$ and Cd^{2+}, which reduced the active sites of Cd^{2+} on the surface of adsorbent. Furthermore, dense hydration shells formed on the surface of adsorbent after adsorption of Na$^+$ could prevent the adsorption of Cd^{2+} on the surface of adsorbent [36].

The removal percentage of Cd^{2+} by BC-FM varied with the pH value of the solution as shown in Fig. 5b. In the range of solution pH 1 ~ 6, the removal percentage increased with the rise of pH. When pH was 1 ~ 4, the change of removal percentage was not obvious and the percentage were all lower than 20%. However, the removal percentage increased sharply from 14.92% to 84.89% when pH changed from 4 to 5. Then when pH changed from 5 to 6, the removal percentage became stable again. It showed that BC-FM was very sensitive to the pH of the solution. A small change in pH might lead to a great change in its adsorption effect on Cd^{2+}, which may be due to the great influence of pH on the surface charge of the adsorbent, resulting in electrostatic attraction or repulsion between the adsorbent and Cd^{2+} [37]. In addition, the adsorption efficiency rose greatly between 4 and 5 of pH values, indicating that the zero-point potential of BC-FM was also very likely in the range of pH 4–5. The pH value corresponding to the zero-point potential is pH$_{zpc}$. When pH < pH$_{zpc}$, the surface of the adsorbent was protonated and showed positive potential, which caused electrostatic repulsion with Cd^{2+}, resulting in poor adsorption effect; On the contrary, when pH > pH$_{zpc}$, the surface of the adsorbent showed negative potential and led to electrostatic attraction with Cd^{2+}, resulting in improved adsorption effect [38].

Obviously, the anion had a small effect on the removal percentage, while the cation had a greater effect on the removal percentage (Fig. 5d). Among all cations, Mg^{2+} had the least effect on the adsorption of Cd^{2+}, while Cu^{2+} had the greatest effect. When there was Cu^{2+} in the solution, the removal percentage of Cd^{2+} reached the minimum value of 24.50%. This indicated that the presence of Pb^{2+}, Cu^{2+} and Zn^{2+} in the polymetallic system had a great influence on the adsorption of Cd^{2+} by BC-FM, and other studies on adsorbent prepared with different materials also showed this property [39–42]. These results could be attributed to the difference in metal properties and the resulting affinity for adsorption sites [39]. Obviously, Pb^{2+}, Cu^{2+} and Zn^{2+} might also readily bind to the adsorption sites on BC-FM.

3.5. Reuse performance and separation of BC-FM

The repeated adsorption–desorption experiment results of BC-FM are shown in Fig. 6a. Compared with the fresh material (adsorbent without adsorption of cadmium ions), adsorption capacity gradually decreased with the increasing numbers of cycles. The reasons might be that the pore structure of BC-FM changed with the desorption process. The decrease of surface adsorption sites leads to the decrease of adsorption capacity. In addition, the weakening of functional groups on BC-FM during desorption also contributed to the decrease of adsorption capacity [43]. After 5 cycles, the adsorption capacity of Cd^{2+} by BC-FM could still reach 81.9% of fresh adsorbent. And after 2 cycles, the adsorption capacity of BC-FM retained 89.4% of that of fresh adsorbent, which indicated that BC-FM had stable and sustainable adsorption capacity for Cd^{2+}. Effective separation and regeneration could improve the economic benefit of adsorbent in practical application. The magnetic hysteresis loops of BC-FM indicated that its saturation magnetization was 10.86 emu g^{-1} (Fig. 6b). The magnetic sensitivity of BC-FM allowed it to be easily separated within 20 s, this was also conducive to its reuse.

3.6. Adsorption mechanism

The above characterization and adsorption experiments illustrated that the adsorption mechanism of BC-FM for cadmium in water was not a single chemical adsorption or physical adsorption, but a multi-mechanism adsorption including physical and chemical action. SEM-EDS and BET results showed that the specific surface area and pore volume of BC-FM were greater than eggshell adsorbent before modification, which enhanced the surface (physical) adsorption capacity of Cd^{2+}. Pseudo-first-order and pseudo-second-order models also showed the interaction of
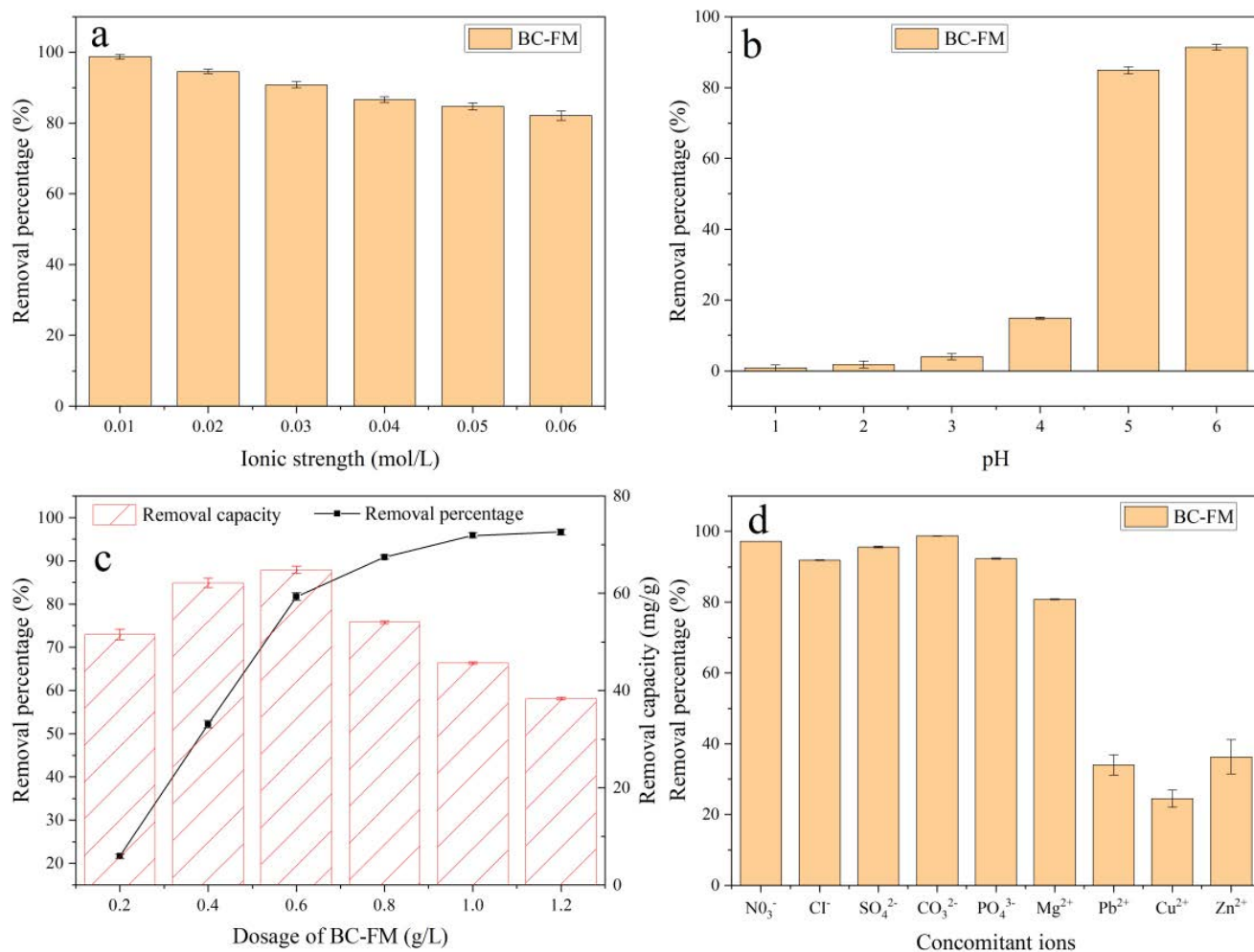
Fig. 5. Effects of ionic strength (a), pH (b), dosage (c) and concomitant ions (d) on the adsorption of contaminants by BC-FM.

chemical and physical mechanisms in the adsorption process, and the diffusion in particles was the main rate-limiting step, which was related to the mesopore structure of BC-FM, such as narrow cracks. FTIR results demonstrated that the oxygen-containing functional groups (–OH, C–O) and magnetic Fe-O on the surface of BC-FM adsorbed Cd^{2+} through complexation [44]. XRD results further indicated that the magnetic material containing Fe–O was maghemite γ-Fe_2O_3. In addition, due to the addition of NaOH during the preparation of BC-FM, $Fe(OH)_3$, and –Fe–O–OH might be generated on the surface of adsorbent [45], which further combined with the oxygen-containing functional groups on the surface of BC-FM at high temperatures to generated iron-containing compounds –Fe–R–COOH and –Fe–R–OH for adsorption of Cd^{2+} [46]. The results of isothermal adsorption fitting further indicated that the monolayer chemical adsorption and multilayer physical adsorption of Cd^{2+} occurred on the surface of BC-FM. The experimental results of influencing factors suggested that the pH of the solution, ionic strength and the existence of other metal cations could make a great influence on the adsorption capacity. pH will change the surface charge of the adsorbent, and high concentration of sodium ions and other

metal ions will also hinder the electrostatic interaction between the surface charge of adsorbent and heavy metals in the solution. This indicated that there was a strong electrostatic interaction between BC-FM and Cd^{2+}. In general, the main mechanisms of adsorption of Cd^{2+} onto BC-FM were surface adsorption (including pore filling), strong electrostatic interaction and complexation of oxygen-containing functional groups (C–O) and compounds containing Fe (Fe_3O_4, –Fe–R–COOH and –Fe–R–OH).

4. Conclusion

Using eggshell as raw material, the magnetic adsorbent successfully prepared by $FeSO_4$ and magnetic modification had a good adsorption effect on Cd^{2+} in aqueous. And its adsorption capacity was 10 times that of the original eggshell adsorbent. Magnetite γ-Fe_2O_3 was successfully loaded onto the surface of adsorbent. The particle size of modified BC-FM became smaller, and the specific surface area and total pore volume were significantly increased. The experimental results of BC-FM adsorption kinetics accorded with the pseudo-second-order kinetics model, and the Langmuir adsorption isotherm could fit the adsorption equilibrium
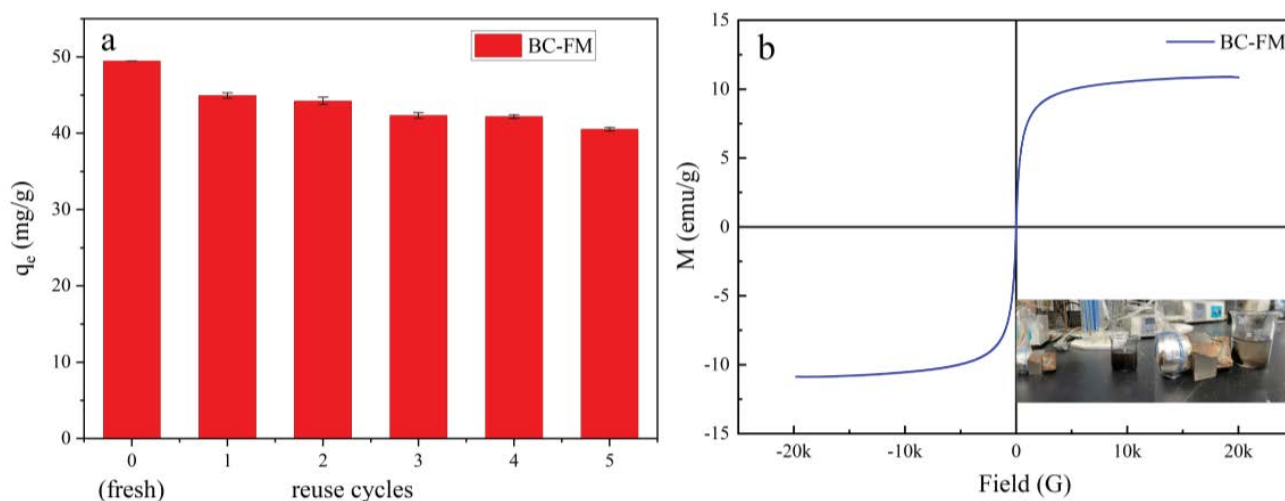
Fig. 6. Cyclic adsorption performance (a) and magnetization curve of BC-FM (b).

well. The optimal dosage was 0.6 g L^{-1}, receiving the largest removal capacity of 64.82 mg g^{-1}. pH and the competitive adsorption of Mg^{2+}, Pb^{2+}, Cu^{2+} and Zn^{2+} were important factor affecting the adsorption process. The lower pH and a certain concentration of metal cation reduced the removal percentage of Cd^{2+}. The main adsorption mechanisms were surface adsorption, strong electrostatic interaction and complexation of oxygen-containing functional groups and compounds containing Fe. BC-FM had good regenerative adsorption capacity and can be recycled after proper treatment.

Disclosure statement

No potential conflict of interest was reported by the author(s).

References

[1] X. Wang, W. Cui, M. Wang, Y. Liang, G. Zhu, T. Jin, X. Chen, The association between life-time dietary cadmium intake from rice and chronic kidney disease, Ecotoxicol. Environ. Saf., 211 (2021) 111933, doi: 10.1016/j.ecoenv.2021.111933.
[2] Y. Ma, D. Ran, X. Shi, H. Zhao, Z. Liu, Cadmium toxicity: a role in bone cell function and teeth development, Sci. Total Environ., 769 (2021) 144646, doi: 10.1016/j.scitotenv.2020.144646.
[3] Suhani, S. Sahab, V. Srivastava, R.P. Singh, Impact of cadmium pollution on food safety and human health, Curr. Opin. Toxicol., 27 (2021) 1–7, doi: 10.1016/j.cotox.2021.04.004.
[4] D.L. Knoell, T.A. Wyatt, The adverse impact of cadmium on immune function and lung host defense, Semin. Cell Dev. Biol., 115 (2020) 70–76.
[5] J. Wu, X. Dong, Y. Zheng, J. Zhang, Progress in molecular mechanism of cadmium carcinogenesis, Asian J. Ecotoxicol., 10 (2015) 54–61.
[6] A.J. Malin, R.O. Wright, The Developmental Neurotoxicity of Cadmium, W. Slikker, M.G. Paule, C. Wang, Eds., Handbook of Developmental Neurotoxicology, 2nd ed., Academic Press, New York, 2018, pp. 407–412.
[7] M. Waisberg, P. Joseph, B. Hale, D. Beyersmann, Molecular and cellular mechanisms of cadmium carcinogenesis, Toxicology, 192 (2003) 95–117.
[8] D. Purkayastha, U. Mishra, S. Biswas, A comprehensive review on Cd(II) removal from aqueous solution, J. Water Process Eng., 2 (2014) 105–128.
[9] Z. Peng, X. Lin, Y. Zhang, Z. Hu, X. Yang, C. Chen, H. Chen, Y. Li, J. Wang, Removal of cadmium from wastewater by magnetic zeolite synthesized from natural, low-grade molybdenum, Sci. Total Environ., 772 (2021) 145355, doi: 10.1016/j.scitotenv.2021.145355.
[10] S. Li, S. Li, N. Wen, D. Wei, Y. Zhang, Highly effective removal of lead and cadmium ions from wastewater by bifunctional magnetic mesoporous silica, Sep. Purif. Technol., 265 (2021) 118341, doi: 10.1016/j.seppur.2021.118341.
[11] K. Pyrzynska, Removal of cadmium from wastewaters with low-cost adsorbents, J. Environ. Chem. Eng., 7 (2019) 102795, doi: 10.1016/j.jece.2018.11.040.
[12] Y. Sun, T. Wang, X. Sun, L. Bai, C. Han, P. Zhang, The potential of biochar and lignin-based adsorbents for wastewater treatment: comparison, mechanism, and application—a review, Ind. Crops Prod., 166 (2021) 113473, doi: 10.1016/j.indcrop.2021.113473.
[13] W. Zhang, L. Xiu, D. Wu, Y. Sun, W. Gu, Y. Zhang, J. Meng, W. Chen. Review and prospect on the structure and physicochemical properties of biochar, Acta Agron. Sin., 47 (2021) 1–18.
[14] T. Varadavenkatesan, R. Vinayagam, S. Pai, B. Kathirvel, A. Pugazhendhi, R. Selvaraj, Synthesis, biological and environmental applications of hydroxyapatite and its composites with organic and inorganic coatings, Prog. Org. Coat., 151 (2021) 106056, doi: 10.1016/j.porgcoat.2020.106056.
[15] V. Vandeginste, Food waste eggshell valorization through development of new composites: a review, Sustainable Mater. Technol., 29 (2021) e00317, doi: 10.1016/j.susmat.2021.e00317.
[16] Y. Feng, B. Ashok, K. Madhukar, J.M. Zhang, J. Zhang, K.O. Reddy, A.V. Rajulu, Preparation and characterization of polypropylene carbonate bio-filler (eggshell powder) composite films, Int. J. Polym. Anal. Charact., 19 (2014) 637–647.
[17] A.S.M. Bashir, Y. Manusamy, Characterization of raw egg shell powder (ESP) as a good bio-filler, J. Eng. Res. Technol., 2 (2015) 56–60.

[18] P.S. Katha, Z. Ahmed, R. Alam, B. Saha, A. Acharjee, M.S. Rahman, Efficiency analysis of eggshell and tea waste as low cost adsorbents for Cr removal from wastewater sample, S. Afr. J. Chem. Eng., 37 (2021) 186–195.

[19] E.R.E. Hassan, M. Rostom, F.E. Farghaly, M.A.A. Khalek, Bio-sorption for tannery effluent treatment using eggshell wastes; kinetics, isotherm and thermodynamic study, Egypt. J. Pet., 29 (2020) 273–278.

[20] X. Li, Y. Qin, Y. Jia, Y. Li, Y. Zhao, Y. Pan, J. Sun, Preparation and application of Fe/biochar (Fe-BC) catalysts in wastewater treatment: a review, Chemosphere, 274 (2021) 129766, doi: 10.1016/j.chemosphere.2021.129766.

[21] T. Ma, C. Yang, X. Jiang, Z. Dang, X. Li, Preparation of nano zero valent iron modified amino biochar and its adsorption and desorption properties for Cd(II), Chin. J. Environ. Eng., 10 (2016) 5433–5439.

[22] Z. Zhu, C.P. Huang, Y. Zhu, W. Wei, H. Qin, A hierarchical porous adsorbent of nano-α-Fe$_2$O$_3$/Fe$_3$O$_4$ on bamboo biochar (HPA-Fe/C-B) for the removal of phosphate from water, J. Water Process. Eng., 25 (2018) 96–104.

[23] Y. Yang, Y. Zhang, G. Wang, Z. Yang, J. Xian, Y. Yang, T. Li, Y. Pu, Y. Jia, Y. Li, Z. Cheng, S. Zhang, X. Xu, Adsorption and reduction of Cr(VI) by a novel nanoscale FeS/chitosan/biochar composite from aqueous solution, J. Environ. Chem. Eng., 9 (2021) 105407, doi: 10.1016/j.jece.2021.105407.

[24] J. Yuan, Y. Qian, G. Xue, Q. Zhang, Q. Li, Z. Liu, X. Li. Preparation of magnetic carbon from activated sludge by hydrothermal carbonization and removal of Cd^{2+} and Pb^{2+} from water, Environ. Eng. (China), 38 (2020) 55–62.

[25] Y. Feng, P. Liu, Y. Wang, W. Liu, Y. Liu, Y.Z. Finfrock. Mechanistic investigation of mercury removal by unmodified and Fe-modified biochars based on synchrotron-based methods, Sci. Total Environ., 719 (2020) 137435, doi: 10.1016/j.scitotenv.2020.137435.

[26] F. Reguyal, A.K. Sarmaha, W. Gao, Synthesis of magnetic biochar from pine sawdust via oxidative hydrolysis of FeCl$_2$ for the removal sulfamethoxazole from aqueous solution, J. Hazard. Mater., 321 (2017) 868–878.

[27] Y. Ma, Y. Qi, L. Yang, L. Wu, P. Li, F. Gao, X. Qi, Z. Zhang, Adsorptive removal of imidacloprid by potassium hydroxide activated magnetic sugarcane bagasse biochar: adsorption efficiency, mechanism and regeneration, J. Cleaner Prod., 292 (2021) 126005, doi: 10.1016/j.jclepro.2021.126005.

[28] L. Trakal, V. Veselská, I. Šafařík, M. Vítková, S. Číhalová, M. Komárek, Lead and cadmium sorption mechanisms on magnetically modified biochars, Bioresour. Technol., 203 (2016) 318–324.

[29] Y. Xie, X. Yuan, Z. Wu, G. Zeng, L. Jiang, X. Peng, H. Li, Adsorption behavior and mechanism of Mg/Fe layered double hydroxide with Fe$_3$O$_4$-carbon spheres on the removal of Pb(II) and Cu(II), J. Colloid Interface Sci., 536 (2019) 440–455.

[30] K.-W. Jung, B.H. Choi, T.-U. Jeong, K.-H. Ahn, Facile synthesis of magnetic biochar/Fe$_3$O$_4$ nanocomposites using electro-magnetization technique and its application on the removal of acid orange 7 from aqueous media, Bioresour. Technol., 220 (2016) 672–676.

[31] F. Huang, L.Y. Gao, J.H. Deng, S.H. Chen, K.Z. Cai, Quantitative contribution of Cd^{2+} adsorption mechanisms by chicken-manure-derived biochars, Environ. Sci. Pollut. Res., 25 (2018) 28322–28334.

[32] Z. Chen, J. Zhang, L. Huang, Z. Yuan, Z. Li, M. Liu, Removal of Cd and Pb with biochar made from dairy manure at low temperature, J. Integr. Agric., 18 (2019) 201–210.

[33] E.C. Lima, F. Sher, A. Guleria, M.R. Saeb, I. Anastopoulos, H.N. Tran, A. Hosseini-Bandegharaei, Is one performing the treatment data of adsorption kinetics correctly?, J. Environ. Chem. Eng., 9 (2021) 104813, doi: 10.1016/j.jece.2020.104813.

[34] Y. Zhou, X. Liu, Y. Xiang, P. Wang, J. Zhang, F. Zhang, J. Wei, L. Luo, M. Lei, L. Tang, Modification of biochar derived from sawdust and its application in removal of tetracycline and copper from aqueous solution: adsorption mechanism and modelling, Bioresour. Technol., 245 Part A (2017) 266–273.

[35] Y. Li, M.A. Taggart, C. McKenzie, Z. Zhang, Y. Lu, S. Pap, S. Gibb, Utilizing low-cost natural waste for the removal of pharmaceuticals from water: mechanisms, isotherms and kinetics at low concentrations, J. Cleaner Prod., 227 (2019) 88–97.

[36] Y. Xiao, Y. Xue, F. Gao, A. Mosa, Sorption of heavy metal ions onto crayfish shell biochar: effect of pyrolysis temperature, pH and ionic strength, J. Taiwan Inst. Chem. Eng., 80 (2017) 114–121.

[37] X. Dong, L.Q. Ma, Y. Li, Characteristics and mechanisms of hexavalent chromium removal by biochar from sugar beet tailing, J. Hazard. Mater., 190 (2011) 909–915.

[38] S. Zhuang, Y. Liu, J. Wang, Covalent organic frameworks as efficient adsorbent for sulfamerazine removal from aqueous solution, J. Hazard. Mater., 383 (2020) 121126, doi: 10.1016/j.jhazmat.2019.121126.

[39] B.-J. Ni, Q.-S. Huang, C. Wang, T.-Y. Ni, J. Sun, W. Wei, Competitive adsorption of heavy metals in aqueous solution onto biochar derived from anaerobically digested sludge, Chemosphere, 219 (2019) 351–357.

[40] Y.-Y. Wang, Y.-X. Liu, H.-H. Lu, R.-Q. Yang, S.-M. Yang, Competitive adsorption of Pb(II), Cu(II), and Zn(II) ions onto hydroxyapatite-biochar nanocomposite in aqueous solutions, J. Solid State Chem., 261 (2018) 53–61.

[41] J. Deng, Y. Liu, S. Liu, G. Zeng, X. Tan, B. Huang, X. Tang, S. Wang, Q. Hua, Z. Yan, Competitive adsorption of Pb(II), Cd(II) and Cu(II) onto chitosan-pyromellitic dianhydride modified biochar, J. Colloid Interface Sci., 506 (2017) 355–364.

[42] Y. Liu, L. Wang, X. Wang, F. Jing, R. Chang, J. Chen, Oxidative ageing of biochar and hydrochar alleviating competitive sorption of Cd(II) and Cu(II), Sci. Total Environ., 725 (2020) 138419, doi: 10.1016/j.scitotenv.2020.138419.

[43] C.H. Lai, S.L. Lo, H.L. Chiang, Adsorption/desorption properties of copper ions on the surface of iron-coated sand using BET and EDAX analyses, Chemosphere, 41 (2000) 1249–1255.

[44] T. Yang, Y. Xu, Q. Huang, Y. Sun, X. Liang, L. Wang, X. Qin, L. Zhao, Adsorption characteristics and the removal mechanism of two novel Fe-Zn composite modified biochar for Cd(II) in water, Bioresour. Technol., 333 (2021) 125078, doi: 10.1016/j.biortech.2021.125078.

[45] J. Wu, D. Huang, X. Liu, J. Meng, C. Tang, J. Xu, Remediation of As(III) and Cd(II) co-contamination and its mechanism in aqueous systems by a novel calcium-based magnetic biochar, J. Hazard. Mater., 348 (2018) 10–19.

[46] Y. Lin, P. Munroe, S. Joseph, A. Ziolkowski, L. van Zwieten, S. Kimber, J. Rust, Chemical and structural analysis of enhanced biochars: thermally treated mixtures of biochar, chickenlitter, clay and minerals, Chemosphere, 91 (2013) 35–40.